Title
Proximal colon–derived O-glycosylated mucus encapsulates and modulates the microbiota

Journal
Science, 370(6515)

ISSN
0036-8075

Authors
Bergstrom, Kirk
Shan, Xindi
Casero, David
et al.

Publication Date
2020-10-23

DOI
10.1126/science.aay7367

Peer reviewed

HHS Public Access

Author manuscript

Science. Author manuscript; available in PMC 2021 May 19.

Published in final edited form as:

Science. 2020 October 23; 370(6515): 467–472. doi:10.1126/science.aay7367.

Proximal colon-derived O-glycosylated mucus encapsulates and modulates the microbiota

Kirk Bergstrom[#1,2,*], **Xindi Shan**[#1], **David Casero**[3], **Albert Batushansky**[4], **Venu Lagishetty**[5], **Jonathan P. Jacobs**[6], **Christopher Hoover**[1], **Yuji Kondo**[1], **Bojing Shao**[1], **Liang Gao**[1], **Wesley Zandberg**[7], **Benjamin Noyovitz**[7], **J. Michael McDaniel**[1], **Deanna L. Gibson**[2], **Sepideh Pakpour**[8], **Negin Kazemian**[8], **Samuel McGee**[1], **Courtney W. Houchen**[9], **Chinthalapally V. Rao**[9], **Timothy M. Griffin**[4,10], **Justin L. Sonnenburg**[11], **Rodger P. McEver**[1,10], **Jonathan Braun**[3], **Lijun Xia**[1,10,*]

[1]Cardiovascular Biology Research Program, Oklahoma Medical Research Foundation, Oklahoma City, OK 73104, USA.

[2]Department of Biology, University of British Columbia, Okanagan Campus, 3333 University Way, Kelowna, British Columbia, Canada, V1V 1V7.

[3]Inflammatory Bowel and Immunobiology Institute, Cedars Sinai Medical Center, Los Angeles, CA 90048, USA.

[4]Aging and Metabolism Research Program, Oklahoma Medical Research Foundation, Oklahoma City, OK 73104, USA.

[5]The Vatche and Tamar Manoukian Division of Digestive Diseases, Department of Medicine, David Geffen School of Medicine at UCLA, Los Angeles, CA, 90095, USA.

[6]Division of Gastroenterology, Hepatology and Parenteral Nutrition, VA Greater Los Angeles Healthcare System, Los Angeles, CA, 90025, USA.

[7]Department of Chemistry, University of British Columbia, Okanagan Campus, 3333 University Way, Kelowna, British Columbia, Canada, V1V 1V7.

[8]School of Engineering, University of British Columbia, Okanagan Campus, 3333 University Way, Kelowna, British Columbia, Canada, V1V 1V7.

[9]Department of Internal Medicine, University of Oklahoma Health Sciences Center, Oklahoma City, OK 73104, USA.

[10]Department of Biochemistry and Molecular Biology, University of Oklahoma Health Sciences Center, Oklahoma City, OK 73104, USA.

[*]Corresponding Authors: Lijun-Xia@omrf.org; kirk.bergstrom@ubc.ca.

Author Contributions: L.X., K.B. conceived, designed the experiments, interpreted data and wrote the manuscript. K.B., X.S., D.C., A.B., V.L., J.J., B.S., L.G., W.Z., B.N., S.M., M.M. D.L.G., S.P., N.K. performed experiments and analyzed data. J.B., D.C., A.B. H.C., CV.R., T.G., R.P.M. commented on the project and contributed to the manuscript preparation.

Competing Interests: The authors have declared that no conflict of interest exists.

Data and Materials Availability: All sequencing data have been deposited in Gene Expression Omnibus (GSE133257). All other data is available in the main text or Supplementary Materials.

[11]Department of Microbiology and Immunology, Stanford University, School of Medicine, Stanford, CA 94305, USA

[#] These authors contributed equally to this work.

Abstract

Colon mucus segregates intestinal microbiota from host tissues, but how it organizes to function throughout the colon is unclear. Here we reveal that colon mucus consists of two distinct O-glycosylated entities of Muc2: a major form produced by the proximal colon, which encapsulates the fecal material including the microbiota, and a minor form derived from the distal colon, which adheres to the major form. The microbiota directs its encapsulation by inducing Muc2 production from proximal colon goblet cells. In turn, O-glycans on proximal-derived Muc2 modulate the structure and function of the microbiota as well as the transcriptome of the colon mucosa. These studies demonstrate that the proximal colon, by producing O-glycosylated mucus, acts as a master regulator of host-microbe symbiosis.

One Sentence Summary:

O-glycan-rich mucus encapsulates colon microbiota

In mammals, the colon houses a dense and diverse commensal microbiota, which impacts health and disease (1–4). The colon mucus system modulates host-commensal symbiosis (5–10). Mucus is primarily a large polymeric network of mucin-2 in mice and humans (Muc2 or MUC2, respectively), which are heavily O-glycosylated (11–13). An established model is that colon mucus is mainly produced by goblet cells in the distal colon to initially form a single non-mobile inner mucus layer, tightly attached to the epithelium, which segregates microbiota from the colon mucosa (5, 14). The inner mucus layer subsequently becomes a loose mobile outer layer where microbiota reside (14–16). However, how the mucus system forms and functions along the whole colon is unclear.

To address this question, we developed a whole colon imaging method by preparing the entire mouse colon with fecal materials into a coil (Fig. 1A, and fig. S1A–C). The “colon coil” was immediately fixed in Carnoy’s solution and embedded in paraffin (CFPE) (17). To image the origin and composition of colonic mucus, longitudinal sections of the wild-type (WT) colon coil were stained with anti-Muc2 antibody, *Maackia Amurensis* lectin II (MALII, recognizing α2,3-linked sialylated and sulfated glycans) (18), and the general bacterial probe EUB338 (EUB) (Fig. 1A). We unexpectedly found discordant expression patterns of MALII-positive Muc2: MALII was negative in most goblet cells of the proximal colon, weakly positive in a goblet cell subset in the middle colon, and strongly positive in most goblet cells of the distal colon (Fig. 1, A and B). In contrast, the mucus layers (inner and outer) were mostly negative for MALII throughout the colon, except for a previously undescribed minor portion of the inner layer closest to the mucosal surface in the distal colon (fig. S2A). This suggests (i) luminal mucus is mainly derived from the proximal colon, a finding supported by increased size and number of goblet cells and higher *Muc2* expression in the proximal vs. distal colon (Fig. 1C, fig. S2B); and (ii) the inner layer consists of two distinct entities of Muc2 from the proximal or distal colon goblet cells.

Notably, we found that MALII primarily marked sulfated O-glycans on Muc2 (fig. S3). Transcriptome analysis of healthy proximal vs. distal colon via RNA-Seq revealed a significant difference in their gene expression profiles (>1000 genes, including *Muc2*) even among similar cell types including goblet cells. These data underscore the functional uniqueness of these two colon regions (fig. S1D).

Whole colon imaging also demonstrated that the luminal mucus layers were attached to fecal pellets, creating “bacteria-sparse” zones in between fecal pellets, based on bacterial fluorescence in situ hybridization (FISH) staining and droplet digital (dd) PCR for 16S rRNA expression in gDNA isolated from pellet-containing and inter-pellet regions (Fig. 1, D and E, and fig. S2C). This was further demonstrated by colonizing mice with a GFP-tagged gut symbiont *Bacteroides thetaiotaomicron* (*B. theta*^{GFP}) (19) (fig. S4, A and B), which was detected inside mucus-coated fecal pellets but not in the inter-pellet spaces, nor in the tissues (fig. S4, C and D). These data suggest that proximal colon-derived mucus encapsulates bacteria in fecal pellets, which supports findings that the mucus can associate with fecal pellets (20, 21). However, how this mucus coating forms and functions remains unknown. To address this, we first imaged sections of freshly excreted fecal pellets wrapped and embedded in mouse peritoneum to preserve fecal integrity (Fig. 1F). Both Alcian blue and immunofluorescent staining revealed that the mucus structure and segregating functions on excreted fecal pellets were identical to that on fecal pellets in situ within their corresponding colon tissues (Fig. 1, F – I).

To exclude fixation artifacts, we validated the results from CFPE samples by staining unfixed snap-frozen colon tissues and pellets or by two-photon microscopic *ex vivo* imaging of unprocessed tissues and pellets from mice gavaged with fluorescent beads. These analyses confirmed the fecal microbiota encapsulation by native mucus (fig. S2D, and fig. S5).

Further biochemical analysis and glycomics of mucins from different colon regions or fecal pellets revealed the differential glycosylation between proximal and distal colon mucus, and that fecal pellet-derived mucins resembled proximal colon mucins (fig. S6, table S1, and Supplementary Text). Comparison of tissues and fecal pellets from different regions of the colon demonstrated stepwise formation of the fecal-associated mucus layers, with a Muc2^{+}MALII^{-} layer associating with feces first in the proximal colon, followed by addition of a Muc2^{+}MALII^{+} layer in the distal colon coinciding with appearance of Muc2^{+}MALII^{+} goblet cells (fig. S7). The Muc2^{+}MALII^{+} layer likely forms after compression as the fecal mass pushes it against the mucosal wall (fig. S8). The mucus phenotype was reproduced in different inbred and outbred strains of mice of both sexes at different ages (fig. S9A–E), and in rats (fig. S9, F and G). Importantly, a similar mucus barrier layer was detected on the surface of feces from healthy primates (baboons) and humans (fig. S10). In summary, these findings provide new insights into how the main components of the colon mucus are formed in mammals and demonstrate that the previously known inner mucus layer in mice in fact consists of two biochemically distinct layers: a thick Muc2^{+}MALII^{-} layer (hereafter b1 layer) from proximal colon goblet cells, and a thin Muc2^{+}MALII^{+} layer (hereafter b2 layer) from distal colon goblet cells (Fig. 1, H and I). Based on these findings, we redefine the mucus system to reflect their origin, biochemical structures, and function (Fig. 1J): The colon mucus system consists of a proximal colon-derived mucus “niche”, and a “barrier”

layer, the latter composed of a proximal colon-derived b1 layer and a distal colon-derived b2 layer.

We then sought to determine the contribution of the b1 and b2 mucus barrier layers to host-microbiota interactions in the colon. Over 80% of the colon mucin mass is derived from core 1- or core 3-derived mucin-type complex O-glycans (O-glycans) (11, 22, 23). Our previous studies showed that core 1-derived O-glycans, whose synthesis is controlled by core 1 β1,3-galactosyltransferase (C1GalT1), present throughout the murine colon (24, 25), while core 3-derived O-glycans, controlled by core 3 β1,3-N-acetylglucosaminyltransferase (C3GnT), are mainly expressed in the proximal colon (24). However, both types of O-glycans produce diverse structures and are required for a functional mucus system by promoting mucus stability in the presence of microbial proteases (24). To determine the contribution of proximal colon O-glycans to overall mucus function, we generated mice lacking both types of O-glycans preferentially in the proximal colon (TM-DKO^{Prox}) (Fig. 2, A – C, and fig. S11, A – C). This was achieved by using a low dose of tamoxifen (TM) in our previously established *C3GnT*$^{-/-}$*;C1galt1*$^{f/f}$*;VillinCreER*^{T2} mice (fig. S11, B and C) (24, 25). Conversely, administering a high dose of TM to *C1galt1*$^{f/f}$*;VillinCreER*^{T2} mice generated biased deletion of O-glycans in the distal colon (TM-IEC *C1galt1*$^{-/-}$) due to differential expression of core 3-derived O-glycans (high in proximal, low in distal) (Fig. 2, A – C) (24). As a control, high dose TM in *C3GnT*$^{-/-}$*;C1galt1*$^{f/f}$*;VillinCreER*^{T2} mice deleted both type of O-glycans in the proximal and distal colon (TM-DKO) (Fig. 2, A – C, and fig. S11, B and C). Analysis of mucus barrier status in tissues and fecal pellets showed significantly reduced mucus thickness in distal colons of TM-DKO^{Prox} relative to control mice (Fig. 2, B and C). Confocal imaging of TM-DKO^{Prox} colon tissues stained with Muc2, MALII, and EUB338 revealed a thinner mucus barrier characterized by loss of the b1 layer, while the b2 layer remained relatively intact (Fig. 2D). In contrast, WT mice had both b1 and b2 layers, TM-IEC *C1galt1*$^{-/-}$ mice had only a visible b1 layer, and TM-DKO lacked both (Fig. 2D). The loss of the b1 layer, but not a b2 layer, also significantly reduced the overall distance of the microbes to the mucosal tissue (Fig. 2, E and F). These results indicate that proximal colon-derived O-glycans form the b1 layer that is critical for segregating the microbiota from the host tissue.

To confirm fecal pellets were encapsulated by proximal O-glycosylated mucus, we imaged excreted fecal pellets from different mouse models. Our results showed reduction of the mucus coating in both TM-DKO^{Prox} and TM-DKO relative to WT and TM-IEC *C1galt1*$^{-/-}$ mice (Fig. 2, G and H). The mucus barrier defect in the TM-DKO^{Prox} mice was confirmed upon colonization with *B. theta*^{GFP}, which was distributed within a degraded mucus barrier (fig. S12). The loss of the b1 layer in TM-DKO^{Prox} mice was likely caused by impaired stability of the O-glycan-deficient Muc2 in the proximal colon (Fig. 2I) (24). To validate these results, we transplanted mucus-deficient TM-DKO pellets into the proximal colon of WT mice and found a rescue of the b1 and b2 layers on excreted transplanted pellets (fig. S13). Additionally, following gavage with fluorescent beads, two-photon microscopy *ex vivo* imaging demonstrated these beads were sequestered in the mucus-coated pellets within the colon of WT but not TM-DKO mice (fig. S14, A and B). The impaired mucus coating phenotype was recapitulated in TM-DKO^{Prox} mice, indicating the importance of the proximal colon-derived b1 layer in sequestering fecal material (fig. S14, C and D).

To determine the functionality of the b1 mucus layer, we first analyzed *16S rRNA* gene abundance from the inter-pellet tissues by PCR. There was significantly more *16S rRNA* within the inter-pellet tissues of TM-DKO^{Prox} and TM-DKO and to a lesser extent in that of TM-IEC *C1galt1*$^{-/-}$ mice, relative to that of WT littermates (fig. S14, E – G). Furthermore, *ex vivo* imaging revealed a loss of the native mucus layer on freshly excreted TM-DKO pellets vs. WT pellets (fig. S14, H and I). As expected, TM-IEC *C1galt1*$^{-/-}$ mice developed spontaneous colon inflammation due to known intrinsic defects in mucus quality (24, 25) (Fig. 2, J and K, fig. S15 and Supplementary Text). Notably, TM-DKO^{Prox} mice also exhibited mild spontaneous colon inflammation compared to WT (Fig. 2, J and K), supporting a key contribution of the b1 layer to mucosal homeostasis. Spontaneous colitis was more severe in TM-DKO, indicating both b1 and b2 layers contribute to mucosal homeostasis. These results were consolidated using the DSS-induced colitis model (fig. S16). Collectively, our data show that the proximal colon is essential in producing the O-glycosylated mucus that encapsulates the microbiota (fig. S15, and Supplementary Text), limiting it from interacting with the mucosa and causing disease as it migrates distally.

To determine if microbiota regulate the secretion of O-glycosylated mucus in the proximal colon, we compared fecal pellets from WT germ-free (GF) mice with specific pathogen-free (SPF) mice. The fecal mucus coating in GF fecal pellets was marginal relative to SPF fecal pellets (fig. S17), suggesting that the microbiota promotes the formation of mucus. To confirm this, we compared mucus formation in GF mice and their littermates conventionalized with a complex microbiota from an SPF mouse (ExGF), as well as SPF mice and their littermates treated for 3 weeks with broad-spectrum antibiotics (SPF^{Abx}) (Fig. 3A). ExGF mice (day 21 post-colonization, D21) had a robust mucus layer similar to that of SPF mice (Fig. 3, A and B). Like GF mice, SPF^{Abx} had a poorly formed mucus layer (Fig. 3A). However, reconstituting SPF^{Abx} mice with a microbiota (SPF^{Recon}) restored the mucus formation (Fig. 3, A and B). To determine the mucus formation dynamics, we tracked the mucus coating of fecal pellets of ExGF mice at different timepoints after colonization with microbiota. At D7 post colonization, a thicker mucus layer was observed on the fecal pellets relative to D0 from the same mouse (Fig. 3, C and D). Similar findings were reproduced in all ExGF mice (Fig. 3E). It was also recapitulated in ExGF mice mono-associated with *B. theta*^{GFP} (fig. S18), indicating a complex microbiota is not required for microbiota-induced formation of fecal-associated O-glycosylated mucus.

We further probed whether and how microbiota regulate proximal colon goblet cell function. Our results demonstrated that the microbiota induced formation of the b1, but not the b2, mucus barrier layer in tissues and on fecal pellets in ExGF (Fig. 3F) and SPF^{Recon} mice (fig. S19A). Additionally, higher Muc2 expression was observed in ExGF vs. GF proximal colon goblet cells in situ (fig. S19B). Similarly, increased levels of Muc2 were detected in the proximal colon of ExGF (D7) and SPF^{Recon} (D7) mice vs. their GF or SPF^{Abx} littermates (Fig. 3G, and fig. S19C), which was concomitant with increased mucus secretion into the lumen (Fig. 3H, and fig. S19, D and E). Dual Muc2/FISH staining showed this secretion was associated with separation of microbiota away from the tissue (Fig. 3I, and fig. S19D). The increased secretion of mucus was confirmed by glycan metabolic labeling (26) in the SPF^{Recon} vs. SPF^{Abx} mice (fig. S20). These secretory surface of goblet cells resembled sentinel goblet cells, whose secretion is dependent upon mucosal inflammasome signaling

(27). However, we found that mice lacking Caspase 1 and 11 (*Casp1/11*$^{-/-}$), key components of the inflammasome, still had relatively normal mucus secretion (fig. S20B), suggesting an alternative pathway. These studies indicate that the microbiota specifically induces the b1 mucus barrier layer by inducing Muc2 expression and secretion in proximal colon goblet cells. Further, fecal mucus screening revealed that a thin mucus barrier and diffuse luminal *Ulex Europaeus agglutinin* I (UEA1) staining, which primarily marks α1,2 fucosylated glycans including those on Muc2^{+} mucus, was indistinguishable among GF or Abx (antibiotics)-treated conditions, confirming a GF-like state is recapitulated by Abx treatment (Fig. 3J). Upon microbiota reconstitution, the diffuse signal shifted to a clear mucus coat around the fecal pellet only in mouse lines with complex O-glycosylation pathways retained in the proximal colon epithelium (i.e. ExGF, SPF^{Recon}, and TM-IEC *C1galt1*$^{-/-;Recon}$), revealing the importance of the proximal colon in establishing the microbially-induced mucus barrier to encapsulate microbes.

To determine if the impact of the microbe-induced encapsulation of fecal pellets by proximal colon-derived O-glycan mucus on the microbial ecosystem and host responses, we performed systems-level analyses of microbiota composition, metabolic output, and changes in host gene expression in TM-DKO^{Prox} mice and their control littermates with a normalized community (Fig. 4A, fig. S21, A and B, and Supplementary Text). First, we analyzed the microbiota composition by taxonomic classification and quantitation of shotgun metagenomics data from proximal and distal lumen contents. There was no overall differences in α-diversity (fig. S21C); however, taxonomic shifts revealed reproducible genotype-induced changes for several abundant species (fig. S21D). Principal component analysis (PCA) showed that, beyond group-specific features (PC1/2, Fig. 4A), there were differences between TM-DKO^{Prox} communities vs. littermate controls common to all groups (PC3, Fig. 4A, and S21D), independent of colon region. Among PC3-associated taxa reduced in TM-DKO^{Prox} vs. control were *Akkermansia muciniphilia*, a known mucin forager (28), *Turicibacter* sp. *H121,* and *Bifidobacterium pseudolongum* (Fig. 4B). In contrast, the relative abundance of PC3-associated taxa including genus *Bacteroides* including *B. thetaiotaomicron* and *B. ovatus*, and *Ruminococcus champanellensis* family was increased in in TM-DKO^{Prox} vs. control (Fig. 4B, and fig. S21D). These results were recapitulated after fitting the species-level metagenomics counts to a multivariate model testing the genotype effect after correcting for group-specific levels (table S2). Peak-to-trough (PTR) analysis (29) on metagemomes of *Akkermansia muciniphila* and *B. thetaiotaomicron* indicated a contribution of proximally derived O-glycosylated mucins to microbial replication rates (fig. S22A). Thus, although we cannot exclude factors such as inflammation and interactions among microbes on community dynamics, the O-glycan-rich mucus forges a growth promoting and regulatory microenvironment for the encapsulated microbial communities.

Next, to determine the relationship between these altered microbial communities and their functional (i.e. metabolic) output, we performed semi-targeted metabolic profiling by GC-MS of proximal fecal content from control and TM-DKO^{Prox} groups, which detected 50 unique primary metabolites in both groups, with group-specific profiles (fig. S22, B and C). Three metabolites, namely 3-hydroxybutyric acid, 2-oxoglutarate and glucose-6-phosphate, were consistently observed only in the TM-DKO^{Prox} group (fig. S22C). There was a clear

effect of proximal colon O-glycan deficiency on the metabolite profile independent of cage effects (Fig. 4C). In support of this, correlation-based network analysis demonstrated a difference in metabolite-metabolite relationships within pooled control vs. TM-DKO^{Prox} samples (Fig. 4D), with only 27 correlated metabolic pairs found in common between the two networks (Fig. 4E). Furthermore, considerable differences in the networks size and directionality of correlations were observed: the number of negative correlations were 3-fold greater in TM-DKO^{Prox} than the control group (table S3). Taken together, these data reveal a disrupted metabolic landscape in mice lacking complex proximal colon O-glycosylation, which is likely a result of changes in microbial homeostasis.

Finally, we looked at the relationship between the altered microbial ecosystem and host gene expression in both the proximal and distal colons from the same mice. Despite intergroup variability (Fig. 4A), we were able to identify two major impacts of the proximal colon O-glycan loss on the host transcriptome in all groups of mice by RNA-Seq (table S4). First, proximal O-glycan loss led to systemic changes (in both proximal and distal regions) in a set of 53 genes, including many related to cell cycle and epithelial homeostasis (Fig. 4F, figs. S23 and S24, and Supplementary Text). Second, a set of 147 genes involved in the interaction between the microbiome and inflammation were upregulated exclusively in distal colon of TM-DKO^{Prox} mice while the same genes were only marginally or inconsistently regulated in the proximal colon (Fig. 4G and Supplementary Text). Collectively, these studies indicate the proximal colon O-glycans are sufficient to impact the mucosal ecosystem by altering community structure, the metabolome, and transcriptional homeostasis locally and in distal sites.

Lastly, we assessed the role of b1 and b2 layers using *il10*$^{-/-}$ mice, which is an established model of spontaneous microbiota-induced chronic colitis independent of O-glycan deficiency (30). *il10*$^{-/-}$ mice with colitis had an impaired b1 layer, associated with altered proximal colon homeostasis and increased distal mucosal microbial intrusion, even though the b2 layer was present (fig. S25). These findings underscore the importance of the b1 layer in maintaining mucus barrier functions during microbiota-induced colitis.

In summary, our data indicate that the proximal colon-derived O-glycans-rich mucus forms both the niche and a primary barrier that encapsulates fecal materials and provides an enclosed ecosystem for microbiota (fig. S26). This new model represents a major revision of the current mucus system model, which describes a mucus layer locally produced and attached to the distal colon tissue. The fecal-associated mucus provides new insights into microbiota metabolism and composition, and may lead to non-invasive strategies such as fecal mucus screening for disease diagnosis.

Supplementary Material

Refer to Web version on PubMed Central for supplementary material.

Acknowledgments:

We thank Gunnar Hansson and Rodney Newberry for reagents and mice; Paul Kincade for critical comments; Miranda Hart, Mark Rheault, Julien Gibon, Ron Banks, and Abby Norris for technical support. **Funding:** National

Institutes of Health (R01DK085691, GM103441); Oklahoma Center for Adult Stem Cell Research, a program of TSET; and the Stephenson Cancer Center of the University of Oklahoma.

References and Notes:

1. Blanton LV et al., Science 352, 1533 (2016). [PubMed: 27339978]
2. Gensollen T et al., Science 352, 539–544 (2016). [PubMed: 27126036]
3. Hsiao EY et al., Cell 155, 1451–1463 (2013). [PubMed: 24315484]
4. Lloyd-Price J et al., Nature 569, 655–662 (2019). [PubMed: 31142855]
5. Johansson ME et al., Nat Rev Gastroenterol Hepatol 10, 352–361 (2013). [PubMed: 23478383]
6. Martens EC et al., Nat Rev Microbiol 16, 457–470 (2018). [PubMed: 29904082]
7. Tropini C et al., Cell Host Microbe 21, 433–442 (2017). [PubMed: 28407481]
8. Donaldson GP et al., Nat Rev Microbiol 14, 20–32 (2016). [PubMed: 26499895]
9. Chassaing B et al., Cell Mol Gastroenterol Hepatol 7, 157–160 (2019). [PubMed: 30510996]
10. Van der Sluis M et al., Gastroenterology 131, 117–129 (2006). [PubMed: 16831596]
11. Allen A et al., Int J Biochem Cell Biol 30, 797–801 (1998). [PubMed: 9722984]
12. Hang HC et al., Bioorg Med Chem 13, 5021–5034 (2005). [PubMed: 16005634]
13. Kudelka MR et al., Adv Cancer Res 126, 53–135 (2015). [PubMed: 25727146]
14. Johansson ME et al., Proc Natl Acad Sci U S A 105, 15064–15069 (2008). [PubMed: 18806221]
15. Hansson GC, Annu Rev Biochem 89, 769–793 (2020). [PubMed: 32243763]
16. Li H et al., Nat Commun 6, 8292 (2015). [PubMed: 26392213]
17. Johansson ME et al., Methods Mol Biol 842, 229–235. [PubMed: 22259139]
18. Geisler C et al., Glycobiology 21, 988–993 (2011). [PubMed: 21863598]
19. Whitaker WR et al., Cell 169, 538–546 e512 (2017). [PubMed: 28431251]
20. Kamphuis JBJ et al., Sci Rep 7, 8527 (2017). [PubMed: 28819121]
21. Swidsinski A et al., Gastroenterology 135, 568–579 (2008). [PubMed: 18570896]
22. Robbe C et al., Biochem. J. 384, 307–316 (2004). [PubMed: 15361072]
23. An G et al., J Exp Med 204, 1417–1429 (2007). [PubMed: 17517967]
24. Bergstrom K et al., Mucosal Immunol 10, 91–103 (2016). [PubMed: 27143302]
25. Fu J et al., Journal of Clinical Investigation 121, 1657–1666 (2011).
26. Johansson ME, PLoS One 7, e41009 (2012). [PubMed: 22815896]
27. Birchenough GM et al., Science 352, 1535–1542 (2016). [PubMed: 27339979]
28. Ottman N et al., Best Pract Res Clin Gastroenterol 31, 637–642 (2017). [PubMed: 29566906]
29. Korem T et al., Science 349, 1101–1106 (2015). [PubMed: 26229116]
30. Rakoff-Nahoum S et al., Immunity 25, 319–329 (2006). [PubMed: 16879997]

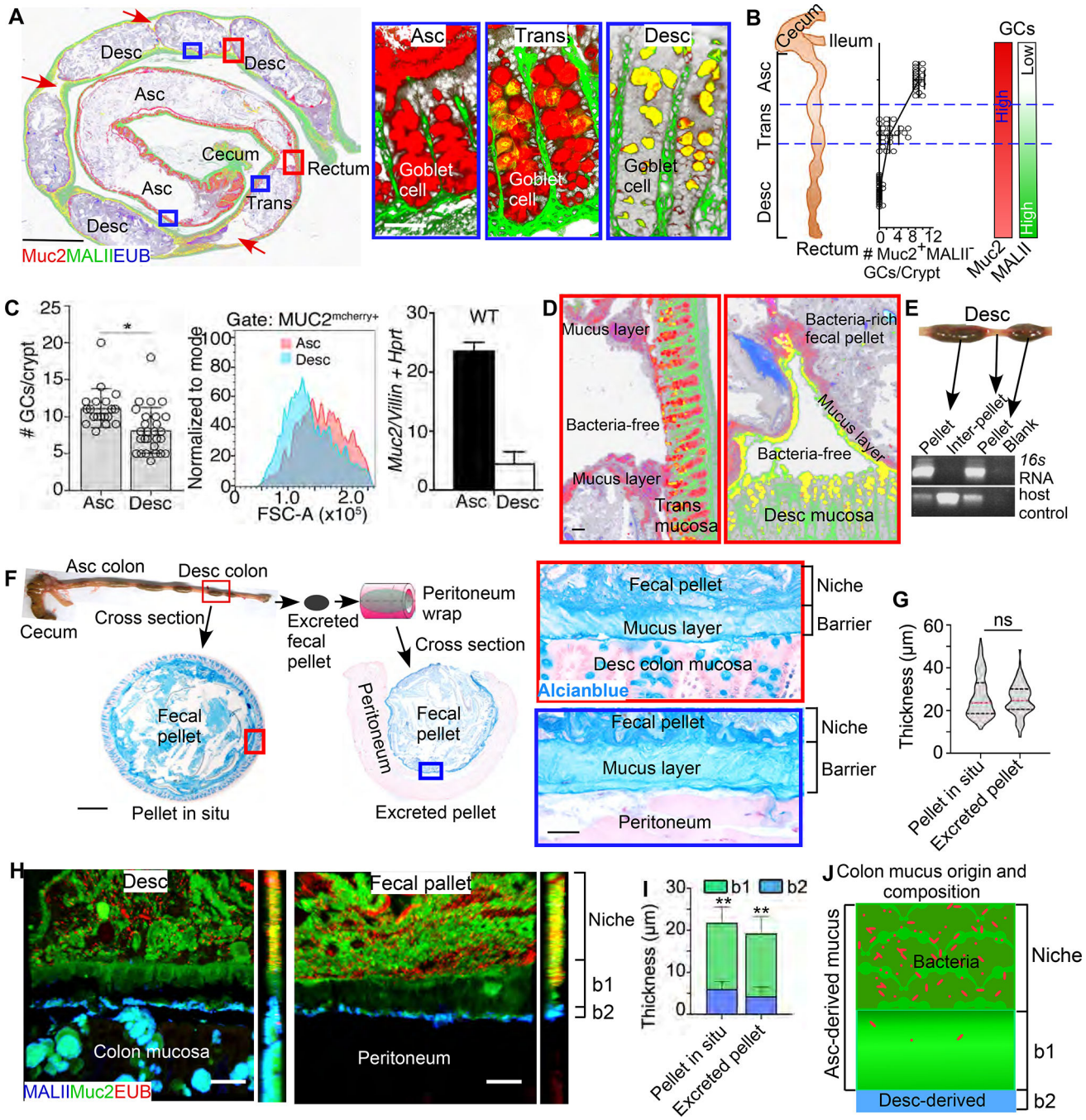

Fig. 1. The proximal colon-derived mucus encapsulates microbiota-containing fecal pellets.

(**A**) Tiled immunofluorescent image of a WT whole colon coil section (left) with goblet cells highlighted (blue boxed images, right). Prox, Mid, and Dis represents proximal, middle, and distal colon, respectively. **(B)** Schematic showing different colon regions (left); $Muc2^{+}MALII^{-}$ goblet cell numbers (GCs, middle); and schematic GC Muc2 and MALII expression profile (right). (**C**) The number of GCs per crypt (left), and *Muc2* expression in colon epithelium (right, qPCR normalized to *villin*). (**D**) Magnified images of red boxed areas in (A). (**E**) ddPCR plot of bacterial *16S rRNA* gene of samples from WT distal colon

with (P) or without pellets (inter-pellet, IP). H_2O, negative control. +, positive control. (**F**) Methods of analyzing mucus on fecal pellets in tissue or excreted fecal pellet wrapped in peritoneum and their Alcian blue-stained images. (**G**) Quantification of mucus thickness stained by Alcian blue (median, red; quartiles, black). (**H**) Z-stacked confocal images of colon cross-sections with pellets or excreted pellets wrapped with peritoneum and corresponding y/z plane (right to each image). Bottom, single-colored images of white-boxed regions. (**I**) Thickness of the mucus layers of (H). (**J**) New model of the mucus layers. The niche and the barrier layer are associated with the fecal pellets. The barrier layer consists of the b1 and b2 layers. The proximal colon produces the niche and the b1 layer. The distal colon forms the minor b2 layer. Scale bars, 4 mm (A); 500 μm (F); 20 μm (A insets, D, F inserts, H). $n \geq 10$ mice, 3 – 5 months old, both sexes. $^{*}P < 0.05$; $^{**}P < 0.01$, vs. b2 layer.

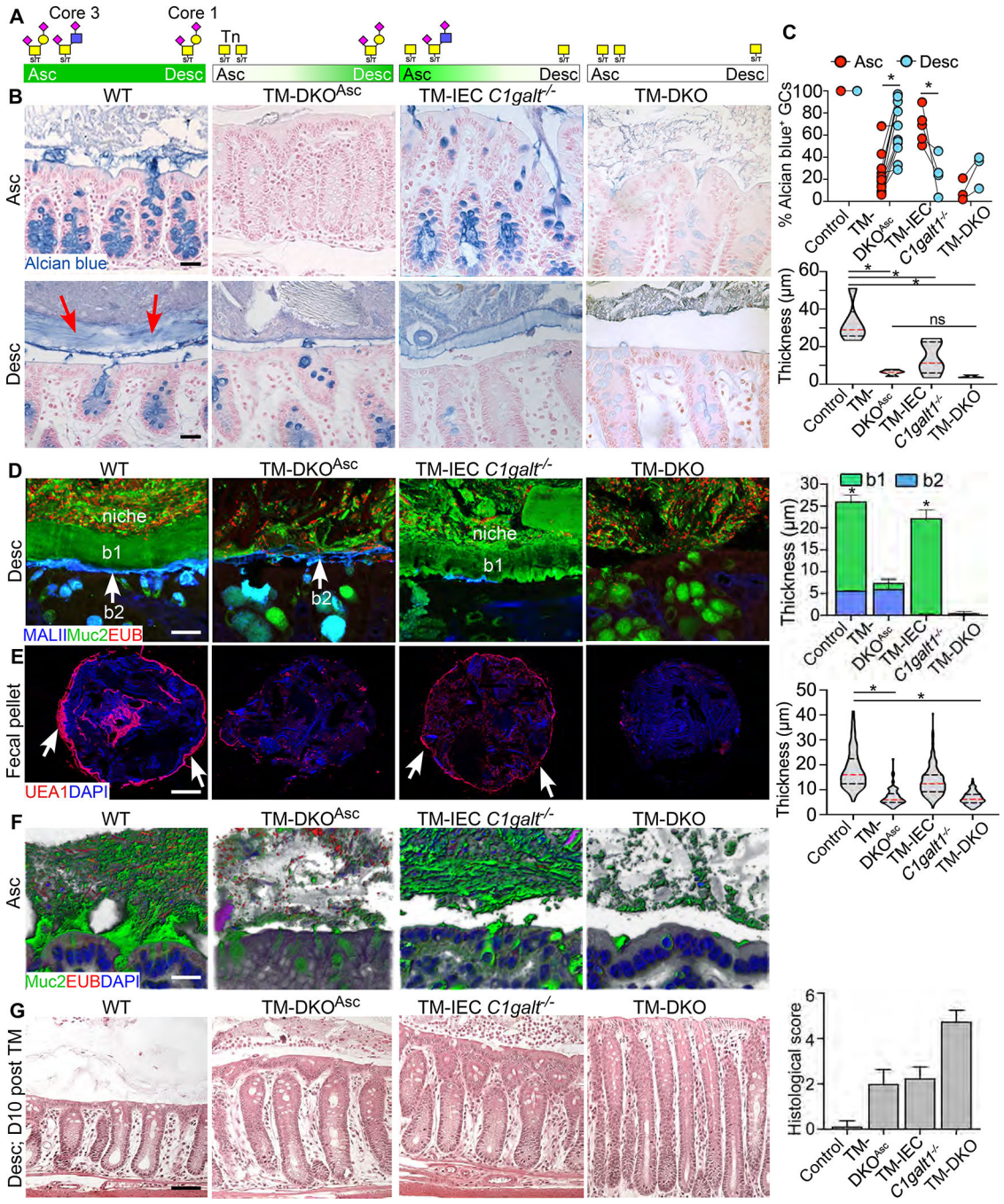

Fig. 2. Proximal colon-derived mucin-type O-glycans govern the composition and function of the mucus barrier.

(**A**) Diagrams depicting simplified forms of core 1- or core 3-derived O-glycans or Tn antigen (GalNAc) in the different colon regions of mouse lines used for results below. (**B**) Representative images of colon sections stained with Alcian blue. Arrows, mucus barrier layer. (**C**) Proportion of Alcian blue^{+} goblet cells in different colon regions (top), and median mucus thickness in distal colons (bottom). (**D**) Z-stack confocal images of colon sections (top). b1, b2, and niche identify the different sublayers of the mucus. (**E**) Mean

mucus thickness in distal colons (D). (**F**) Histogram showing frequency distribution of individual bacterial distances to the bottom of the distal mucosa surface represented in (D). (**G**) Confocal tiling images of cross-sections of fecal pellets stained with the lectin UEA1. Arrows mark the mucus layer. (**H**) Violin plot of mucus thickness of entire mucus layer surrounding the fecal pellet represented in (G). (**I**) Blended Z-stack confocal images of proximal colon cross sections. (**J**) Representative images of H&E-stained colon cross sections. (**K**) Graph depicts histologic colitis scores. $n \geq 5$ mice, 3 – 5 months old, both sexes. Scale bars, 20 μm (B, D, and I); 50 μm (J); 500 μm (G). $*P < 0.05$, as indicated, and vs. b2 layer in (D).

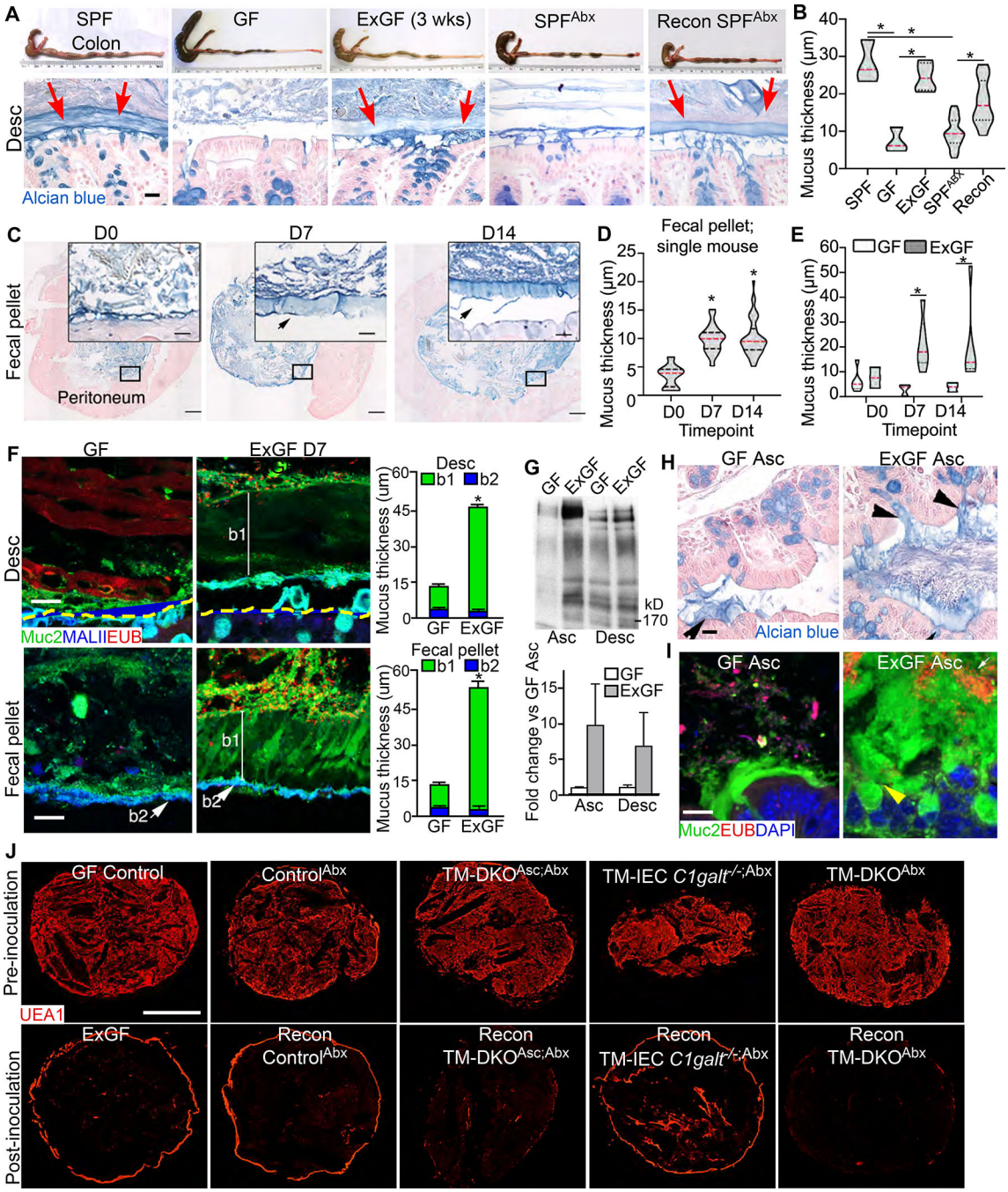

Fig. 3. The microbiota directs its own encapsulation by inducing Muc2 production in the proximal colon.

(**A**) Gross picture of colon (top) and Alcian blue-stained mucus and goblet cells in colon sections (bottom) of mice with and without a complex microbiota. Arrows mark mucus barrier layer. (**B**) Median mucus barrier layer thickness in distal colon sections represented in (A). (**C**) The formation of the fecal mucus barrier over time in ExGF mice. Images show Alcian blue-stained excreted fecal sections. Inset, magnified image of mucus layer (arrows). (**D**) Violin plot of mucus thickness over time in (C). (**E**) Median mucus barrier layer

thickness of excreted feces from multiple ExGF mice. (**F**) Confocal Z-stack images of distal colon (top) and excreted fecal pellet sections (bottom). Arrow, b2 layer. Line, spans thickness of the b1 layer. Right, mean thickness of b1 and b2 layers. (**G**) Western blot of tissue Muc2 separated by composite AgPAGE (top), and densitometry of Muc2 signal (bottom). GAPDH, loading control. (**H)** Alcian blue-stained WT colon sections. Arrowheads mark mucus secretion. (**I**) Confocal Z-stack images of WT colon sections. Arrowheads, secreted mucus. (**J**) Tiled confocal images of excreted fecal pellet sections from mice pre- or post-inoculation with a complex microbiota. Scale bars, 10 μm (C insets); 20 μm (A, F, H, I); 500 μm (C); 1000 μm (J). *$P < 0.05$, as indicated in (B and E), vs. D0 in (D), and vs. GF b1 layer in (F).

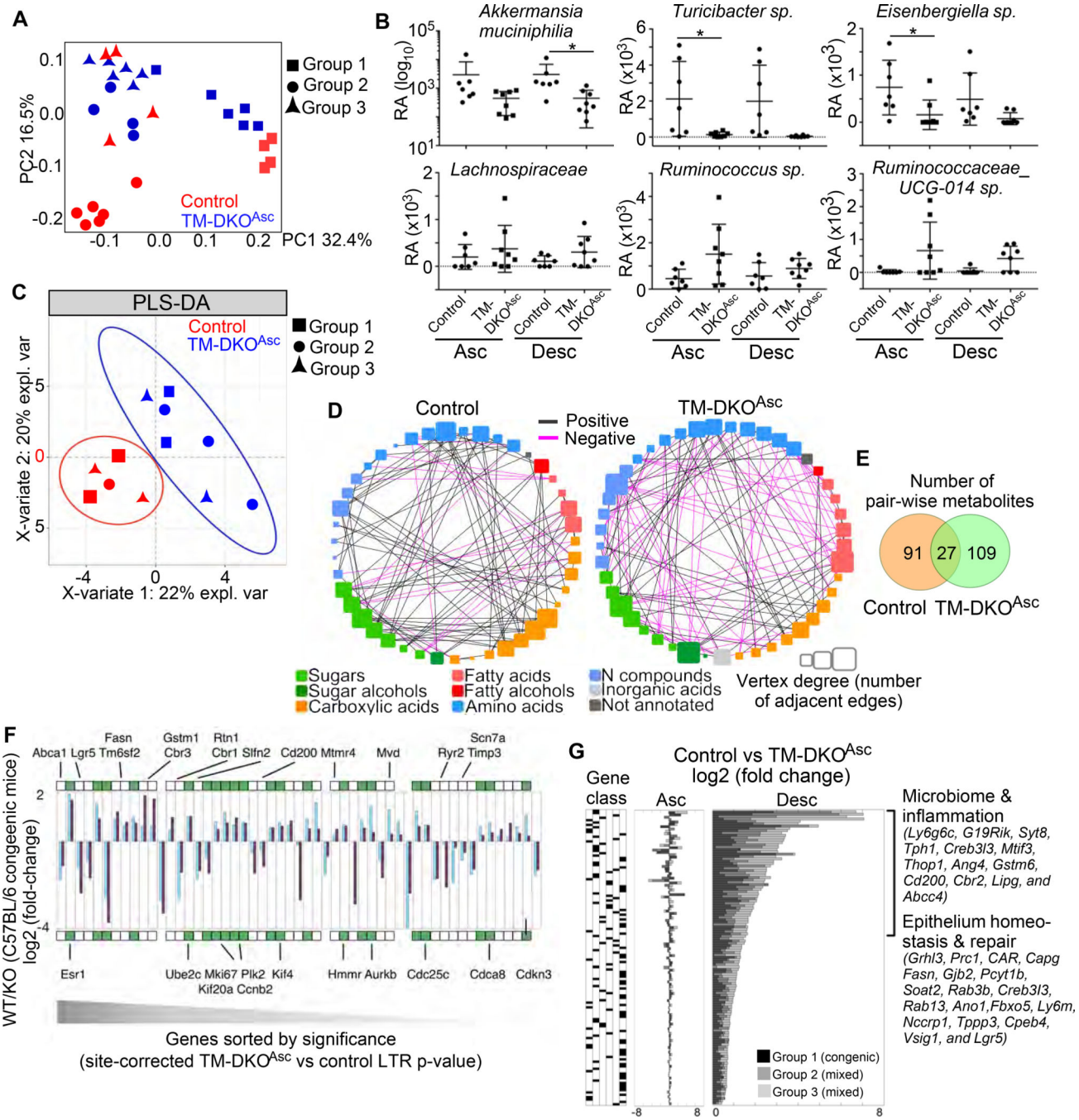

Fig. 4. Loss of O-glycans in the proximal colon alters microbiota community structure and the host mucosal transcriptome throughout the colon.

(A) Principal component analysis (PCA) of species-level counts. The first three principal components (PC1, PC2, PC3) and percent of variance explained are shown. $n = 5$ mice/group. (**B**) Relative abundance for selected taxa showing highest PC3 loadings in **(**A**)**. y axis, variance-stabilized data computed from species-level counts (Bracken classifier). (**C**) Partial Least Squares Discriminant Analysis (PLS-DA) of microbial metabolites. (**D**) Metabolite correlation networks between control ($n = 5$) and TM-DKO^{Prox} ($n = 5$). (**E**) Venn diagram of

pair-wise correlated metabolites. (**F**) Gene expression signature showing 53 significantly different genes between pooled control and TM-DKO^{Prox} mice. For clarity, only Group 1 is shown. Green boxes, maximal enrichment for cell-cycle, proliferation genes (hypergeometric *P*-value<1e-12). Marked boxes, genes governing epithelial function. Genes are sorted (left to right) by significance (LTR *P*-value, table S4). Grey gradient highlights *P*-values in decreasing significance. (**G**) Barplot showing genes uniquely different in TM-DKO^{Prox} distal colon. Left (black/white heatmap): Gene class assigned to each gene according to its expression profile in indicated single-cell epithelial subtypes (black boxes, see Methods); Middle: Barplots of gene expression fold changes in each group of mice for both proximal and distal colon; Right: selected top-ranked genes by global fold-change grouped by their molecular function. $*P < 0.05$, as indicated.